Experimental study and numerical modeling of supercritical carbonation of steel fiber reinforced concrete

Hao Bao[a,b,d], Tan Wang[c], Min Yu[c,*], Ruyu Wang[b], Mohamed Saafi[d], Jianqiao Ye[d,*]

a. Hubei Key Laboratory of Disaster Prevention and Mitigation, China Three Gorges University, Yichang, China

b. College of Civil Engineering & Architecture, China Three Gorges University, Yichang, China

c. School of Civil Engineering, Wuhan University, Wuhan, China

d. School of Engineering, Lancaster University, Lancaster LA1 4YR, UK

* Correspondence author: ceyumin@whu.edu.cn (M. Yu), j.ye2@lancaster.ac.uk (J. Ye)

Abstract: In this paper, supercritical carbonation tests of steel fiber reinforced concrete (SFRC) are carried out. The effects of volume fraction and length-diameter ratio of steel fiber on the carbonation depth of SFRC under supercritical conditions are studied. A novel multi-phase and multi-physics coupling model for supercritical carbonation of SFRC is proposed, which considers random distribution of coarse aggregate, porosity, and steel fibers in SFRC, as well as the distribution of interfacial transition zones (ITZ) between coarse aggregate, steel fibers and cement. The results indicate that the porosity of the SFRC is reduced by 32.3%, and its compressive strength of SFRC increases by 25.1% ~ 42.7% after supercritical carbonation treatment. When the volume fraction of steel fiber is less than 1.5%, the supercritical carbonation depth of the SFRC decreases with the increase of the volume fraction and the length to diameter ratio, respectively. The influence of the ITZ between coarse aggregate and cementitious matrix on the supercritical carbonation depth of the SFRC is found to be 2 to 6.8 times greater than that of the ITZ between steel fibers and cementitious matrix. The average carbonation depth of the SFRC increases gradually with the increase of ITZ thickness and porosity. The effect of ITZ porosity on the supercritical carbonation depth of the SFRC is more significant than that of ITZ thickness.

Keywords: Steel fiber reinforced concrete; Supercritical carbonation; Multi-phase and multi-physics coupling model; ITZ; Carbonation depth.

1. Introduction

Fiber Reinforced Concrete (FRC), recognized as an advanced engineering material, has seen extensive application in civil engineering due to its superior mechanical properties and durability [1, 2]. Compared to the conventional concrete, FRC significantly enhances tensile and flexural strengths as well as toughness by integrating steel fibers into the concrete matrix [3, 4]. This integration reduces brittleness and dry shrinkage deformation [5], delays or prevents cracking [6-8], and refines the microstructure [9, 10]. These improvements offer significant advantages to FRC in applications such as tunnel lining [11], bridge construction, airport runways, and military engineering [12]. For ordinary concrete structures, the migration of CO_2 and the carbonation reaction within the concrete convert $Ca(OH)_2$ into $CaCO_3$. This process lowers the pH of the pore solution, disrupts the passive film on the surface of the steel reinforcement, and ultimately leads to steel corrosion [13, 14]. However, SFRC is a type of cementitious composite material. Upon carbonation infiltration, CO_2 reacts with alkaline substances within the SFRC matrix and the interfacial transition zone (ITZ) between steel fibers and matrix, forming calcium carbonate with a larger molar volume than the original phase [15].

This process potentially reduces the pore volume and permeability of the concrete matrix and ITZ [16]. The addition of steel fibers into the concrete matrix can enhance its compactness and increase resistance to CO_2 penetration [17, 18], thereby improving the carbonation resistance of the concrete [19]. The enhancement of carbonation resistance in concrete due to steel fibers is primarily attributed to the reduction of plastic shrinkage cracks and the decreased porosity [20-22]. During the carbonation reaction in a steel fiber concrete, the resulting $CaCO_3$ fills the pore spaces [23, 24], thereby reducing porosity and CO_2 diffusion capability, which in turn decreases the carbonation reaction rate [21].

Accelerated carbonation has been widely used to study carbonation properties of fiber-reinforced concrete [25]. This process accelerates carbonation by increasing CO_2 concentration and controlling environmental conditions such as temperature and humidity. Although accelerated carbonation shortens the time compared to natural carbonation, it still takes several months to reach the desired carbonation depth [26, 27]. In recent years, with the advancement of CO_2 storage technology [28], supercritical carbonation has attracted attention as an emerging research method. This technique has been applied to treat cementitious materials [29-33] and heavy metal seals [34-36]. When the temperature and pressure exceed 304.12 K and 7.38 MPa, respectively, CO_2 exists in a supercritical fluid state [37] with gas-liquid two-phase characteristics. This state significantly enhances the diffusion and reaction rates of CO_2 within the concrete, thereby accelerating the carbonation process [38, 39]. Supercritical carbonation technology has become a promising, time- and labor-saving method in the study of carbonation resistance for fiber-reinforced concrete. In addition, supercritical carbonation of fiber-reinforced concrete can significantly increases the strength and toughness of the material [40, 41], improves pore size distribution [41], enhances permeation resistance [42], alters chemical and structural properties of the concrete [39], reduces porosity, and increases material density [43, 44]. However, the addition of steel fibers can increase the pathways for CO_2 penetration, reduce matrix density, and consequently decrease the carbonation resistance of SFRC. It was found that adding steel fibers can change carbonation rate of concrete, as observed in [20] that adding a volume fraction of 1.5% steel fibers result in the slowest carbonation rate [20]. However, when the volume fraction was increased to 2%, the carbonation rate accelerated [20, 45]. Thus, the optimal content of steel fiber remains a subject of debate.

Compressive strength and carbonation depth are primary indicators used to evaluate carbonation performance of SFRC treated with supercritical CO_2 [46, 47]. Supercritical carbonation of SFRC is a complex physicochemical process involving multi-physical field, coupling chemical reaction rate equations, mass conservation equations, kinetic energy conservation equations, and energy conservation equations. Various factors such as porosity, water content saturation, liquid permeability, and gas permeability influence the depth of supercritical carbonation [40, 46]. Additionally, SFRC is a non-homogeneous material composed of phases like coarse aggregate, cement matrix, steel fibers, micropores, and interfacial transition zones, all of which affect the supercritical carbonation depth and compressive strength of SFRC. Consequently, supercritical carbonation of SFRC is a multifaceted multiphase and multi-field coupled physicochemical reaction process. Currently, both experimental and numerical simulation studies on the supercritical carbonation of ordinary concrete exist. Yu et al. conducted an experimental study on the supercritical carbonation of concrete and proposed a multi-field coupled model that considers physicochemical processes such as carbonation reaction, gas-liquid two-phase flow in the porous medium, and CO_2 dissolution and diffusion in water [23, 48]. To characterize the distribution of coarse aggregate, porosity, and interfacial transition zone in concrete, a concrete multiphase model was proposed to investigate the effects of these factors on the depth of supercritical carbonation [38]. However, there are few studies on the supercritical carbonation of SFRC [23], and the strengthening mechanism of SFRC through supercritical carbonation treatment remains uncertain.

To elucidate the carbonation mechanism and properties of SFRC under supercritical CO_2 conditions, supercritical carbonation tests are conducted on SFRC with varying mix ratios. The changes in micro-morphology, porosity and compressive strength of SFRC specimens before and after supercritical carbonation are analyzed. Based on the previous work [38, 46], in this paper, a multifield coupling model for the supercritical carbonation of SFRC is established. To accurately represent the random distribution of coarse aggregate, porosity, and steel fibers in SFRC, as well as to account for the interfacial transition zone between the coarse aggregate, steel fibers, and the cementitious matrix, a multiphase model of SFRC is proposed. Utilizing this multifield coupling model for supercritical carbonation and the multiphase model of SFRC, a multiphase and multi-field coupling model of SFRC supercritical carbonation is developed. This model is capable of simulating the effects of multiple parameters, including aspect ratio of steel fibers, volume fraction of steel fibers, thickness and porosity of the interfacial transition zone between coarse aggregate and steel fibers, on the depth of supercritical carbonation in SFRC.

2. Experimental investigation

2.1. Raw materials and mix proportion

In accordance with the specifications for the mix proportion design of ordinary concrete [49] and the standard test methods for fiber reinforced concrete [50], the targeted compressive strength of steel fiber-reinforced concrete (SFRC) is set at 40 MPa. The cement utilized in the experiments is sourced from Ezhou, Hubei, and is classified as P.O 42.5 ordinary Portland cement. The coarse aggregates range in size from 5 to 20 mm, with continuous grading, a mud (silt/clay) content of 0.41%, and bulk and specific densities of 1429 kg/m^3 and 2797 kg/m^3, respectively. The fine aggregates consist of natural river sand, with a fineness modulus of 2.70 and bulk and specific densities of 1398 kg/m^3 and 2549 kg/m^3, respectively. A polycarboxylic acid high-performance water-reducing agent produced by Foshan Xinqi Tuoda New Materials Group Co., Ltd, with a water reduction rate of 30%, was used. The respective design mix proportions of the SFRC are presented in Table 1. Shear wave steel fibers with the length-diameter ratios of 30, 60, 80, manufactured by Wuhan Hansen Steel Fiber Limited Liability Company, were used to prepare the SFRC specimens. The physical and mechanical properties of the steel fibers are shown in Table 2.

Table 1

Mix proportions of concrete.

Cement (kg/m^3)	Coarse aggregate (kg/m^3)	Fine aggregate (kg/m^3)	Water (kg/m^3)	Water-binder ratio
445	1078	732	178	0.40

Table 2

Physical and mechanical properties of steel fibers.

Equivalent diameter (mm)	Density (g/cm^3)	Length-diameter ratio	Length (mm)	Tensile strength (MPa)	
0.55	7.8	30, 60, 80	16.5, 33, 44	1120	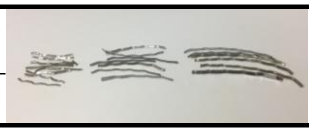

2.2. Specimen preparation

The performance of steel fiber-reinforced concrete is profoundly influenced by two pivotal factors: volume fraction and length-diameter ratio of steel fibers. To study carbonation performance of SFRC under supercritical conditions, a range of fiber volume fractions, namely 0%, 0.5%, 1%, and 1.5% with length-diameter ratios of 30, 60, and 80 are considered. The design of the SFRC specimens is outlined in Table 3.

Table 3

Design details of SFRC specimens.

Specimen	Length-diameter ratio, λ	Volume fraction, ρ	Slump (mm)
SFRC-L60-V0.0	60	0	34
SFRC-L60-V0.5	60	0.5%	32
SFRC-L60-V1.0	60	1.0%	31
SFRC-L60-V1.5	60	1.5%	30
SFRC-L30-V1.5	30	1.5%	32
SFRC-L80-V1.5	80	1.5%	28

Note: In Table 2, the numbers after L and V are the length-diameter ratio and steel fiber volume fraction, respectively, of a SFRC.

Slump is one of the methods for assessing the workability of SFRC. To ensure the workability of SFRC [50], the slump of the SFRC specimens was assessed using a standard slump cone. The slump cone was placed on a non-absorbent rigid horizontal base plate. The mixed SFRC was poured into the cone in three layers of thickness, each filling approximately one-third of the cone's height. Each of the layers underwent 25 compaction cycles. Once the final layer was poured and settled, the slump cone was lifted straight up within 5 seconds, allowing the concrete to settle freely. The slump values for each type of the SFRC were determined by measuring the vertical distance between the highest point of the concrete and the original cone height using a ruler, as shown in Table 3.

To investigate the carbonation properties of the SFRC with varying length-diameter ratios and volume fractions under supercritical CO_2 conditions, SFRC cubes with a side length of 100 mm are manufactured. Six sets of nine SFRC cubes each are made according to the specifications outlined in Table 3. Among the nine specimens of each group, three of them are tested before carbonation and another three are tested after carbonation for compressive strength. The remaining three are tested for carbonation depth. To ensure a uniform dispersion of steel fibers in the concrete and prevent fiber clumping, the mixing process followed the mix proportions of concrete in Tables 1 and the design details in Table 3. First, the aggregates, cement, and water were mixed thoroughly for 2 minutes. Next, the steel fibers were added gradually during the mixing process until all the fibers were added. This was finished by an additional 3 minutes mixing to ensure best possible uniformity. The thoroughly mixed concrete is then poured into molds. A vibration table is used to shake the molds to release any bubbles that may form in the pouring process. After casting, the molds are transferred to a wet room cured for 24 hours before being demolded. The specimens are subsequently cured in a standard curing room with a temperature of (20±2)℃ and humidity of (95±3)% for 28 days. To maintain a relative humidity of 70% within the SFRC specimens, the cured SFRC specimens are placed in a temperature and humidity-controlled chamber for an additional 28 days.

2.3. Supercritical carbonation test

To assess the performance of SFRC under supercritical CO_2 conditions, a closed-cycle supercritical carbonation system is employed as shown in Fig. 1. The system operates by compressing air with an air compressor to propel a booster pump. Simultaneously, the booster pump continuously compresses and propels the gas from the CO_2 cylinder into the reaction chamber until the pressure and temperature in the reaction chamber surpass 7.38 MPa and 31.2°C, respectively. At this point, the CO_2 in the reaction chamber is in a supercritical state, enabling supercritical carbonation of SFRC. Further details on the closed-cycle supercritical carbonation system for cementitious materials can be found in the authors' previous research [51].

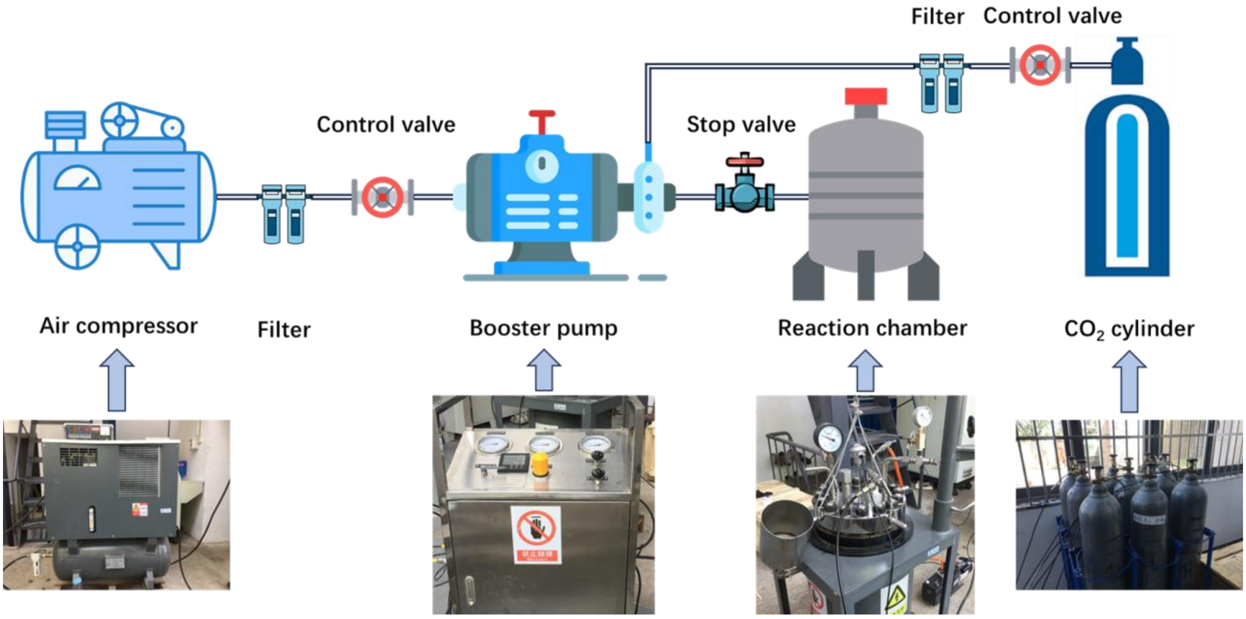

Fig. 1. Equipment connection diagram for supercritical carbonation system.

The supercritical carbonation process of the SFRC employing a closed-cycle supercritical carbonation system is primarily structured into four distinct test phases: test preparation, CO_2 boosting, CO_2 holding, and CO_2 recycling. The operational steps are summarized below:

(1) Test preparation phase

1.1) Six specimens are positioned within the reaction chamber, and the lid of the reaction chamber is securely tightened.

1.2) The CO_2 cylinders are linked to the CO_2 gas source inlet of the booster pump, and the high-pressure CO_2 outlet of the booster pump is connected to the gas delivery port of the chamber. At this stage, all the switches on both the chamber and the booster pump are switched off, and the chamber is vacuumed until an approximate pressure of -1.00 bar is reached.

(2) CO_2 boosting phase

2.1) All switches on reaction chamber, booster pump, and CO_2 cylinder are activated to allow CO_2 being pumped into the reaction chamber driven by the pressure difference. The pressures in the reaction chamber and the CO_2 cylinder are closely monitored and documented until equilibrium is reached between the two.

2.2) The throttle valve controlling the driving gas on the top of the booster pump is adjusted continuously to allow a continuous flow of CO_2 into the chamber until the pressure reaches the designated target.

2.3) The temperature inside the reaction chamber is continuously regulated to attain the specified temperature through water circulation and a heating rod.

(3) CO_2 holding phase

3.1) Once the pressure and temperature inside the reaction chamber has reached the designated levels, the CO_2 cylinder, booster pump, and all switches on the reaction chamber are deactivated.

3.2) The fluctuations in temperature and pressure in the reaction chamber are closely monitored and documented. In the event of a decline in air pressure in the chamber, the booster pump is reactivated. CO_2 injection into the reaction chamber resumes until the target pressure is reached again.

3.3) Supercritical carbonation of the SFRC takes place under the designated holding pressure and temperature, for the specified carbonation time.

(4) CO_2 recycling phase

4.1) Upon completion of the supercritical carbonation test for the SFRC, all valves are closed. Subsequently, the gas outlet of the reaction chamber is connected to the inlet of the CO_2 gas source on the booster pump, followed by connecting the CO_2 gas outlet of the booster pump to the CO_2 gas cylinder.

4.2) All the switches on the CO_2 cylinder, booster pump, and chamber are opened. The CO_2 from the gas chamber is injected into the cylinder due to the pressure difference.

4.3) Upon achieving equilibrium between the pressures within the chamber and the CO_2 cylinder, the control valve at the booster pump is tuned to introduce the CO_2 from the chamber into the cylinder, thereby initiating the process of CO_2 recovery.

Throughout the supercritical carbonation of the SFRC, the predetermined pressure and temperature are maintained at 8.0 MPa and 40°C, respectively. The total carbonation time is 7.2 hours, including 6 hours supercritical carbonation time. The air pressure and temperature in the reactor are recored at 10-minute intervals encompassing CO_2 pressurization, CO_2 holding pressure, and CO_2 recovery phases. Upon the conclusion of the supercritical carbonation test, the six specimens are extracted from the reaction chamber. Fig. 2 illustrates the temperature and pressure profiles of select specimens during the supercritical carbonation test, which shows that the designed carbonation system is capable of consistently regulating the internal pressure and temperature of the reaction chamber by the closed-cycle supercritical carbonation process.

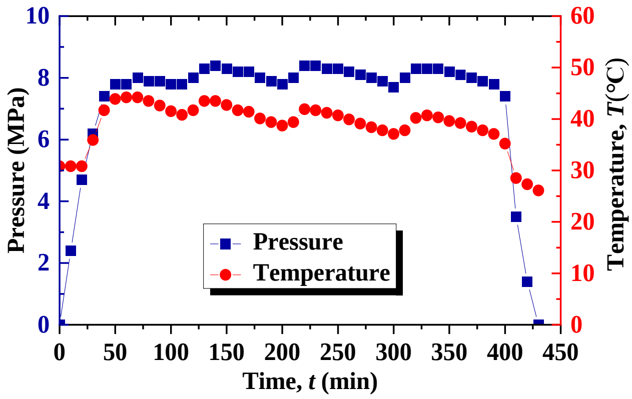

(a) SFRC-L60-V0.0 and SFRC-L60-V0.5

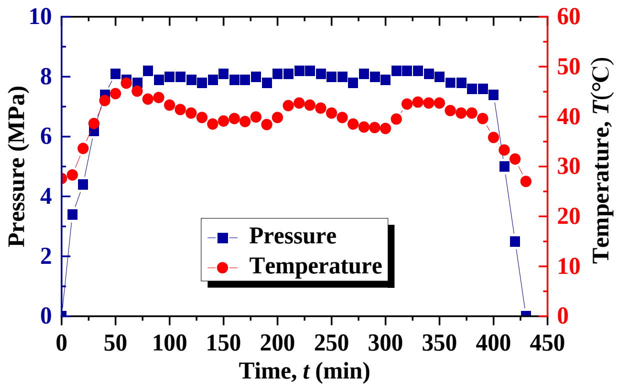

(b) SFRC-L60-V1.0 and SFRC-L30-V1.5

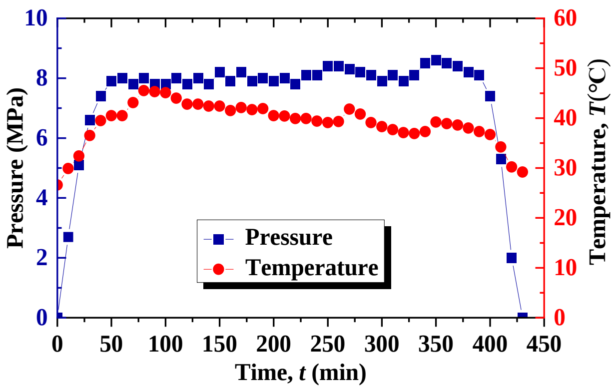

(c) SFRC-L60-V1.5 and SFRC-L80-V1.5

Fig. 2. Temperature and pressure in the reaction chamber during supercritical carbonation.

2.4. Compressive strength testing

After completing the supercritical carbonation test on the SFRC specimens, selected samples are prepared for compressive strength testing. The compressive strength of the SFRC specimens before and after supercritical carbonation is measured using a 3000 kN MTS YAW6306 testing machine, following the standard steel fiber reinforced concrete test method (CECS 13:2009) [50]. The loading rate is 1.2 MPa/s. The test system automatically records the applied load, including the ultimate load, and the corresponding displacements.

2.5. Carbonation depth measurement

After completing supercritical carbonation process, the SFRC specimens are removed from the reactor. Each specimen is then halved at an appropriate cutting speed to prevent fiber pullout and detachment of the interface between the cement matrix and the fibers. The surfaces of cuts are properly cleaned before phenolphthalein solution, a pH indicator, is uniformly sprayed over the cuts. The chemical reaction shows pink in alkaline (non-carbonated) concrete, while remaining colorless in areas where carbonation has occurred. The carbonation profiles of the specimens are obtained using an image scanner [23], and the mean and standard deviation of carbonation depth are then measured.

2.6. Microscopic analysis

2.6.1. SEM test

To explore alterations in the micro-morphology of SFRC after supercritical carbonation and investigate the influence of steel fibers on the depth of carbonation, Microscopic images of the SFRC samples, both before and after supercritical carbonation, are taken and examined to study the micro-morphological features, such as steel fibers, matrix, interfacial transition zones (ITZs), and cracks, using a scanning electron microscope (SEM, JEOL JSM-7800F). Before observation, the carbonated SFRC samples were precisely cut, broken, and cleaned to ensure that the test samples retained the steel fibers and the matrix. This was done to minimize the potential interference of dust on the carbonation results of the SFRC. The samples are dried up to the same weight in an oven, and their surfaces are coated with ion-sputtered gold powder to increase electrical conductivity. Subsequently, the samples are examined by the SEM to observe the microstructure of both the matrix and the steel fibers in the samples.

2.6.2. MIP test

To evaluate the impact of supercritical carbonation on the pore structure of concrete, mercury pressure tests are carried out on specimens before and after supercritical carbonation using a mercury piezometer (AutoPore IV 9500). Before the MIP test, samples with and without being super-critically carbonated is randomly chosen from those that has been examined by SEM. The samples are immersed in anhydrous ethanol to arrest hydration and subsequently sealed to prevent further carbonation. The specimens are then subjected to MIP test to study their pore size distribution, and changes in concrete porosity due to supercritical carbonation.

3. Numerical simulation

3.1. Multiphase model of SFRC

3.1.1. Random porosity model

To characterize the stochastic and inhomogeneous distribution of porosity within SFRC, and to account for the correlation in the spatial distribution of porosity, it is assumed that the porosity follows a lognormal distribution. Eq. (1) provides the equation for the spatial correlation function employed to describe the random distribution of porosity in SFRC.

$$\phi(x, y) = \exp\left[-\left(\frac{x^2}{a^2} + \frac{y^2}{b^2}\right)^{\frac{1}{1+r}}\right] \tag{1}$$

where a and b represent the autocorrelation lengths, assumed to be 0.01 m for both a and b [51], and r stands for the roughness coefficient, set to 0 in this paper. The Fourier transform and inverse Fourier transform of Eq. (1) are employed to formulate the stochastic porosity model for SFRC. Further insights into the procedure for generating the random porosity model can be found in Yu [48].

3.1.2. 2D random steel fibers and aggregates model

For the grading and proportion of coarse aggregates in SFRC, the Monte Carlo method is employed to generate circular aggregates randomly within specified space, from which the coordinates of the center and the area of each circular aggregate are determined. A polygonal Voronoi diagram is then created using the center of each circular aggregate as a control point. Utilizing the vertices of each of the polygonal Voronoi cells as the points for interpolation, closed B-spline curves are generated by connecting the vertices. For crushed stone aggregates, convex polygons are created by selecting nodes from the closed B-spline curves. The area is proportionally scaled down to ensure equivalence between the area of the resulting rubble and the area of the initially generated circular aggregate at the corresponding location. Based on the diameter, length, and quantity of steel fibers, the Monte Carlo method is applied also to randomly position steel fibers in the above generated aggregate model. Steel fibers are subsequently repositioned if collisions with aggregates occur. This process leads to the establishment of a two-dimensional random steel fibers and aggregates model for SFRC. Further details regarding the generation of the random aggregate model can be found in Bao [52].

A multiphase model, which can characterize random distribution of matrix porosity, coarse aggregate, and steel fibers in concrete is developed by the following steps: (1) incorporate the measured average porosity of the matrix into the porosity random distribution model for microscopic characterization of the random distribution of matrix porosity; (2) utilize the mix ratio, the generated aggregate and steel fibers and the characteristic parameters of SFRC as input for the random aggregate and fiber distribution model of concrete; and (3) ultimately establish a multiphase model of SFRC that considers porosity, recycled aggregate, and steel fiber distribution. The method for establishing the multiphase model of SFRC is illustrated in Fig. 3.

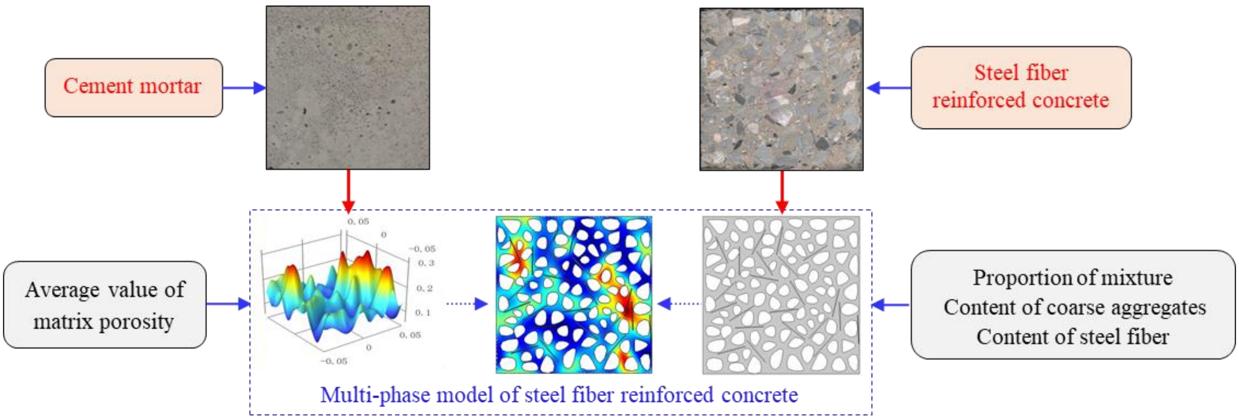

Fig. 3. Flow chart of multi-phase modeling method of SFRC.

3.1.3. Distribution of ITZs around coarse aggregates and steel fibers

An ITZ exists between the coarse aggregate, steel fibers, and cement matrix [53, 54]. The presence of this ITZ also impacts the distribution of supercritical carbonation depth of concrete. To study the impact of the ITZ between coarse aggregate and steel fibers on the supercritical carbonation depth, a multiphase model is developed, encompassing the ITZs of both coarse aggregate and steel fibers. The distribution model of the ITZ is proposed based on the random model of steel fibers and aggregates.

The process of ITZ generation is as follows: (1) Initially, the vertex coordinates of each convex polygon of the coarse aggregate and the four vertex coordinates of the steel fibers are obtained. (2) Subsequently, the boundary of each convex polygon of the coarse aggregate and the rectangular steel fiber is expanded parallel to the original boundary by a distance equivalent to the thickness of the ITZ. (3) The region between the extended coarse aggregate boundary and the original boundary constitutes the ITZ of the coarse aggregate, while the region between the extended steel fiber boundary and its original boundary forms the ITZ of the steel fiber. Fig. 4 illustrates the distribution of the ITZ surrounding the coarse aggregate and steel fibers, each with a thickness of 100 μm.

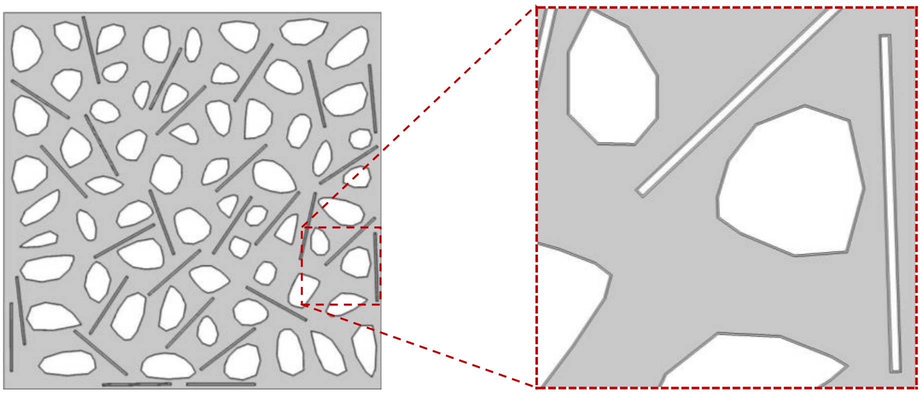

Fig. 4. Distribution of the ITZ surrounding the coarse aggregates and steel fibers.

3.2. Multi-physics coupling model for supercritical carbonation of SFRC

Supercritical carbonation of SFRC is a complex multi-physics coupled reaction process. In order to describe the transport and reaction process of supercritical CO_2 in SFRC, a supercritical carbonation model for SFRC is established based on previous study [23]. The model considers processes such as the carbonation reaction between CO_2 and $Ca(OH)_2$, gas and liquid flow in porous media, dissolution and diffusion of CO_2 in the pore water film, and heat transfer in porous media. Darcy's law was employed to describe the permeation process of CO_2 in SFRC under different carbonation conditions. Finally, a multi-physics coupled theoretical model for the supercritical carbonation of SFRC is established. The development of the model is illustrated in Fig. 5.

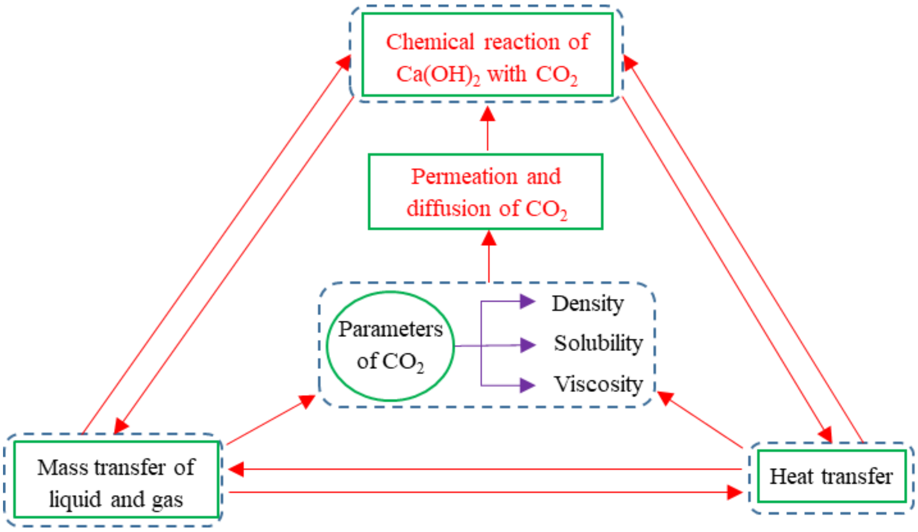

Fig. 5. Flow chart of multi-physics coupled modeling method for supercritical carbonation of SFRC.

The governing equations for the supercritical carbonation of SFRC are presented in Eqs. (2-6). The mathematical model considers the chemical reaction rate, conservation of mass in gas-liquid two-phase flow, diffusion and dispersion of CO_2 in water, conservation of energy in porous media, and solubility of CO_2 in water.

$$\frac{\partial R_c}{\partial t} = \alpha_1 \times f_1(h) \times f_2(g_v) \times f_3(R_c) \times f_4(T) \tag{2}$$

$$\frac{\partial (g)}{\partial t} = \frac{\partial (m_{co_2})}{\partial t} \tag{3}$$

$$\frac{\partial (n S_\alpha \rho_\alpha)}{\partial t} + \nabla \cdot (\rho_\alpha \vec{u}_\alpha) = q_\alpha \tag{4}$$

$$\vec{u}_\alpha = -\frac{k_0 \left(\frac{n}{n_0}\right)^3 \cdot \left(\frac{1-n_0}{1-n}\right)^2 k_{r\alpha}}{\mu_\alpha} (\nabla P_\alpha - \rho_\alpha \vec{g}) \tag{5}$$

$$\left(\rho C_q\right)_{eff} \frac{\partial T}{\partial t} = \nabla \cdot \left(k_{eff} \nabla T\right) - \left(C_g \rho_g \vec{u}_g + C_w \rho_w \vec{u}_w\right) \nabla T \tag{6}$$

where: R_c represents the degree of carbonation; g denotes the mass concentration of CO_2 in water; n signifies the decrease in porosity of the material during carbonation; P_α denotes the pressure in phase α, with the subscript α referring to the liquid phase (w) and the gas phase (g). Additional information about other parameters can be found in Zha [46] and Yu [48].

To solve Eqs. (2-6), the following initial and boundary conditions for the supercritical carbonation of SFRC, as outlined in Eqs. (7-9), are considered.

$$R_c = R_{c0} = 0,\ P_g = P_{g0},\ P_w = P_{w0},\ g = g_0 = 0,\ T = T_0,\ t = 0\ on\ \Omega \tag{7}$$

$$\vec{n} \cdot \nabla R_c = 0,\ \vec{n} \cdot \nabla g = 0\ on\ \Gamma_2 \tag{8}$$

$$P_g = P_{g,sur},\ P_w = P_{w,sur},\ T = T_{sur}\ \ on\ \Gamma_1 \tag{9}$$

where: R_{c0} denotes the initial condition of carbonation degree; P_{g0} and P_{w0} represent the initial water pressure and the initial air pressure, respectively; g_0 indicates the initial dissolved concentration of CO_2 in water; T_0 is the initial temperature; $\vec{n}$ is the normal vector of the boundary; Γ_2 and Γ_1 are the boundaries using Neumann's and Dirichlet's conditions, respectively; $P_{g,sur}$ and $P_{w,sur}$ denote the surrounding gas and liquid pressures, respectively; and T_{sur} is the ambient temperature. Details of the other parameters can also be found in Zha [46] and Yu [48].

3.3. Multi-phase and multi-physics coupling model for supercritical carbonation of SFRC

The multi-phase model and the multi- physics coupling model of supercritical carbonation of SFRC are integrated to formulate the multi-phase and multi-physics coupling model for supercritical carbonation in SFRC. SFRC can be considered as a porous medium material consisting of coarse aggregates, steel fibers, a cement matrix, and pores. The random aggregates and steel fibers model is utilized to describe the distribution of coarse aggregates and steel fibers in SFRC, respectively. The input parameters of the model, such as the mix proportion, the coarse aggregate content, and the volume fraction and length to diameter ratio of steel fibers, are Section 2.1 and 2.2.

The transport and reaction of CO_2 in the SFRC are influenced by the material properties, such as the initial porosity and intrinsic permeability, that need to be determined for the multi-phase and the multi-physics coupling supercritical carbonation model. Specifically, the initial average porosity of the cement matrix is determined through the MIP test, as illustrated in Table 4. The temperature and pressure data obtained during the supercritical carbonation test of the SFRC specimens are incorporated into the numerical carbonation model. The mean and variance of the carbonation depth are statistically analyzed by comparing the carbonation depth distribution obtained from both the supercritical carbonation test and the multi-phase model and the multi- physics coupling model. The multi-phase model and the multi-physics coupling model for supercritical carbonation of SFRC is then calibrated and refined.

Table 4

Main characteristic parameters of SFRC materials.

Item	Value	References
Intrinsic permeability, k_0	1.5×10^{-20} m^2	[55]
Capillary pressure curve coefficient, α	5.3695×10^{-8} Pa^{-1}	[56]
Relative permeability coefficient, m	0.4396	[56]
Relative humidity, h_0	0.70	Measured
Initial porosity, n_0	14.7%	Measured

4. Results and discussion

4.1. Compressive strength of SFRC under supercritical carbonation

Fig. 6 presents the compressive strength of SFRC with a water-cement ratio of 0.4 before and after supercritical carbonation, considering different volume fraction and length to diameter ratio of steel fiber. Specifically, Fig. 6(a) and Fig. 6(b) illustrate the effects of volume fraction and length to diameter ratio on the compressive strength of SFRC before and after supercritical carbonation, respectively. Before supercritical carbonation, the compressive strength of the SFRC is increased by 2.6%, 12.5%, and 18.4% when steel fibers of 0.5%, 1.0%, and 1.5% in volume fraction is, respectively, added to the concrete. When the length to diameter ratio of the steel fibers is 60 and 80, the respective compressive strength of the SFRC is 9.5% and 11.3% higher than when the ratio is 30. This enhancement can be attributed to the bridging effect of steel fibers within the concrete matrix, which restrains crack initiation and propagation under loading, thereby improving load-bearing capacity [57, 58]. After supercritical carbonation, the compressive strength of the SFRC shows a significant increase of 25.1% ~ 42.7% compared to that before carbonation. This improvement is likely due to the deposition of $CaCO_3$ within internal pores and at the ITZs between steel fibers and the cement matrix [59]. The filling of these voids densifies the SFRC matrix and ITZs, thereby enhancing its overall compressive strength.

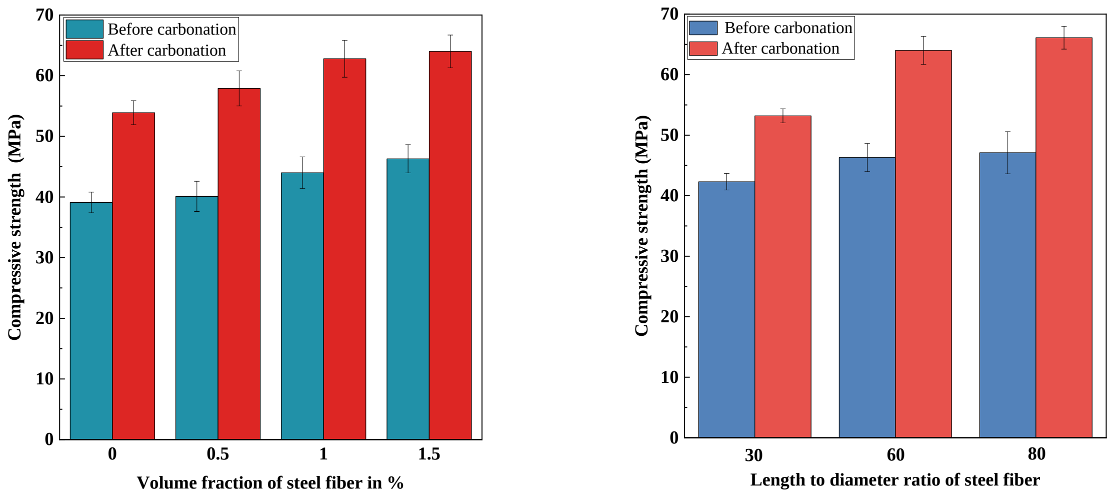

(a) Effect of volume fraction (b) Effect of length to diameter ratio

Fig. 6. Effect of volume fraction and length to diameter ratio of steel fiber on the compressive strength of SFRC.

4.2. Microstructure evolution of SFRC under supercritical carbonation

4.2.1. Morphology evolution of SFRC

The microstructure of the cementitious matrix and cracks before and after supercritical carbonation of the concrete without steel fibers are shown in Fig. 7a and b at a magnification of 1000 times. It can be observed that micro-cracks and tiny pores are present within the matrix before carbonation (Fig. 7a). However, although micro-cracks and small pores still exist within the matrix after carbonation, both their quantity and size are reduced, and the cement matrix as a whole is denser (Fig. 7b). This indicates that the porosity or cracks inside the matrix can be reduced by supercritical carbonation treatment. To evaluate the evolution of the SFRC microstructure before and after supercritical carbonation treatment, the SFRC specimen (SFRC-L60-V1.5) with a volume fraction of 1.5% is selected for the analysis. To observe the steel fibers, cracks, and the cement matrix simultaneously under the scanning electron microscope (SEM), a magnification factor of 200 is chosen. The SEM images of SFRC-L60-V1.5 before and after supercitical carbonation are shown in Fig. 7 (c) and (d), respectively. It can be observed that micro-cracks appear along the narrow gap between the matrix and the steel fibers in the non-carbonated samples. Although cracks are also observed in the area between the matrix and steel fibers in the carbonated samples, the crack length is reduced, and the matrix and steel fibers are firmly bonded together. This suggests that porosity or cracks between the matrix and steel fibers can be reduced by supercritical carbonation. The weakness of the interfacial transition zones (ITZs) between cement matrix and fibers [10, 60] and between cement matrix and aggregate [38] may serve as a shortcut for CO_2 transport, which leads to a more rapid carbonation in the ITZ. In addition to the porosity, coarse aggregate and ITZ, the presence of steel fibers in the SFRC may also contribute to the stochastic nature of the carbonation boundaries.

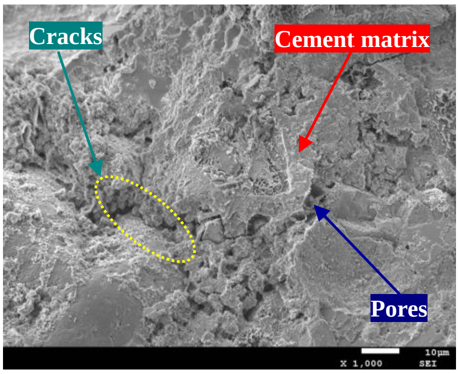

(a) SFRC-L60-V0.0 before carbonation

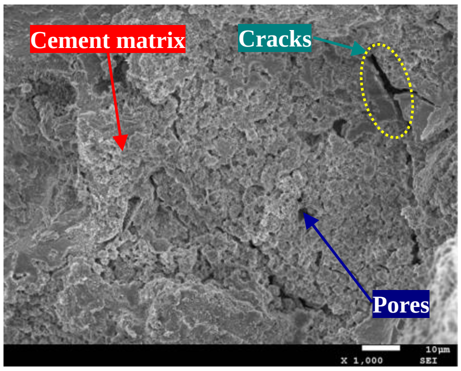

(b) SFRC-L60-V0.0 after carbonation

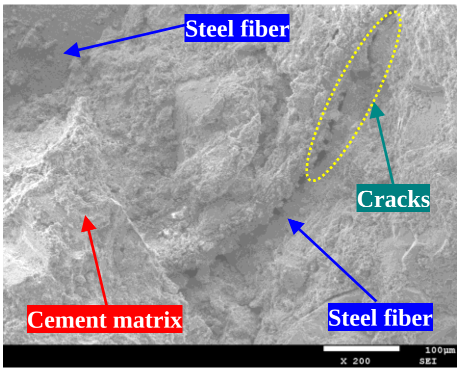

(c) SFRC-L60-V1.5 before carbonation

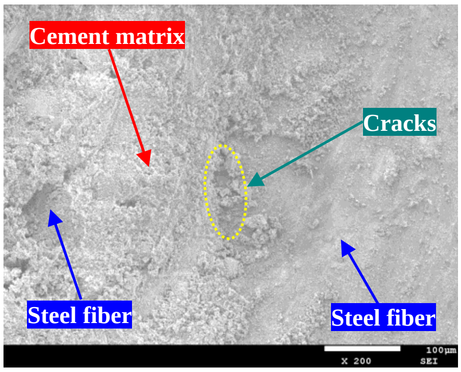

(d) SFRC-L60-V1.5 after carbonation

Fig. 7. SEM images of SFRC with and without steel fibers before and after supercritical carbonation.

4.2.2. Porosity variation of SFRC

To evaluate the change in porosity of the SFRC before and after supercritical carbonation and to calibrate the parameters for the numerical model, Mercury Intrusion Porosimetry (MIP) tests are conducted on the SFRC matrix before and after supercritical carbonation. The obtained Mercury porosimetry curves for SFRC-L60-V1.5 are shown in Fig. 8. The porosity of the SFRC matrix before supercritical carbonation treatment is 14.7%, and the porosity after treatment is 9.1%. The porosity of the SFRC after supercritical carbonation treatment is reduced by 32.3%. This reduction is primarily due to the reaction of $Ca(OH)_2$ and C-S-H in the pores of the cement matrix with CO_2 to form $CaCO_3$, which blocks the pore structure [61]. The initial average porosity and the coefficient of variation of porosity are 14.7% and 0.4 [51], respectively, and these two parameters will be input to the numerical model.

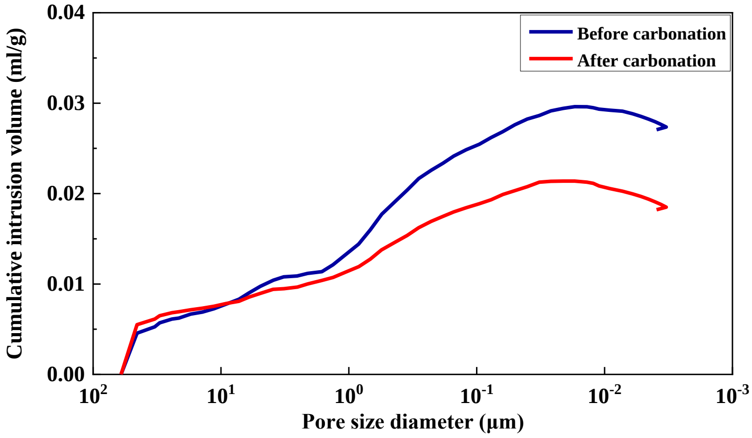

Fig. 8. Mercury porosimetry curves for SFRC-L60-V1.5 before and after supercritical carbonation.

4.3. Experimental supercritical carbonation results of SFRC and validation of numerical models

4.3.1. Supercritical carbonation depth of SFRC

In order to elucidate the variation of carbonation depth of the SFRC under supercritical CO_2 conditions, the carbonation depth of the SFRC specimens is measured and analyzed. The carbonation contours of selected SFRC specimens are illustrated in Fig. 9. It is evident that the randomness of concrete carbonation boundaries can be influenced not only by the random distribution of coarse aggregate and matrix pores [51, 52] but also by the presence of steel fibers.

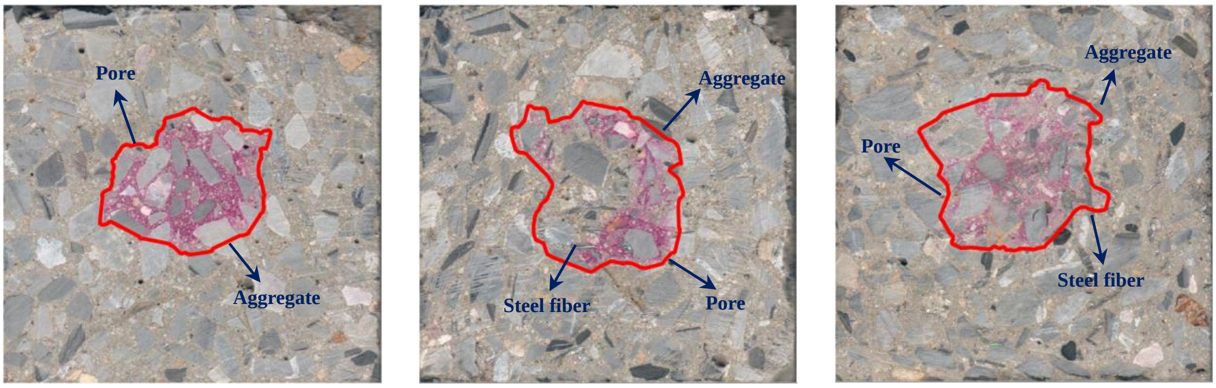

(a) SFRC-L60-V0.0 (b) SFRC-L60-V0.5 (c) SFRC-L60-V1.0

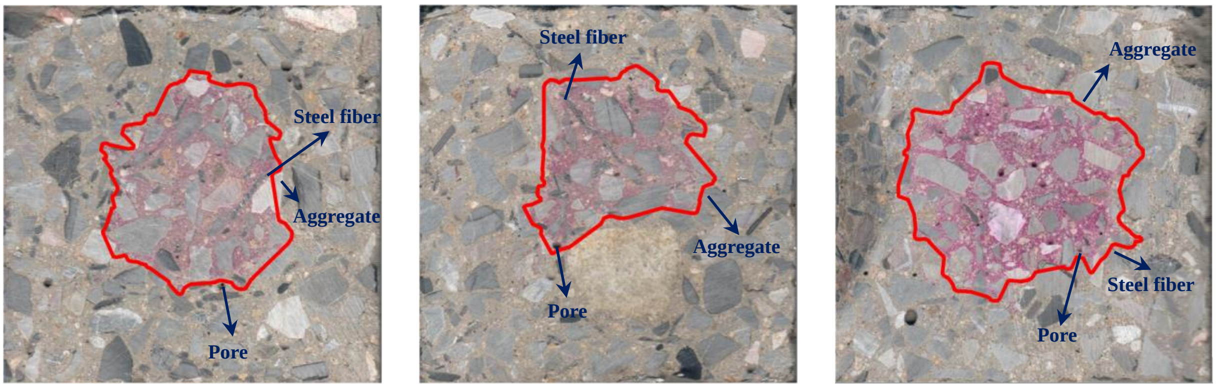

(d) SFRC-L60-V1.5 (e) SFRC-L30-V1.5 (f) SFRC-L80-V1.5

Fig. 9. Supercritical carbonation depth distribution of SFRC with different volume fraction and length-diameter ratio of steel fibers.

To assess the impact of steel fibers on carbonation within the SFRC, MATLAB R2014a for statistical analysis of carbonation depth in cementitious materials is utilized for the statistical analysis of supercritical carbonation depth. The statistical analysis of SFRC carbonation depth distribution curves along the carbonation area is shown in Fig. 10. Fig. 10 (a) shows the distribution curves of the carbonation depth along the carbonation area, where the horizontal lines are the average. The results of average, maximum, minimum carbonation depth and variance of carbonation depth of the SFRC are shown in the table in Fig. 10 (b). The mean values of carbonation depth and coefficient of variation after completion of the supercritical carbonation tests on the SFRC specimens are shown in Table 5.

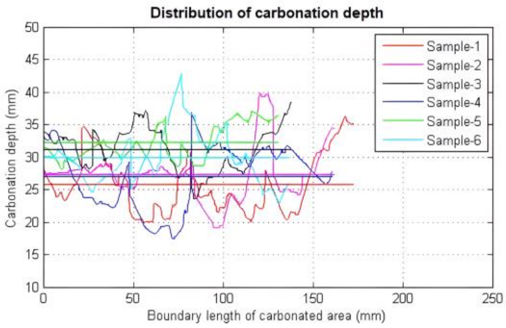

(a) Distribution curves of carbonation depth

Statistical results on the carbonation depth of cementitious materials

	Average value (mm)	Maximum value (mm)	Minimum value (mm)	Variance (mm2)
Sample-1	25.7172	36.2288	19.9153	19.6612
Sample-2	27.2709	39.8169	19.2220	16.6891
Sample-3	31.1499	38.4279	23.5808	11.1544
Sample-4	27.0550	36.7713	17.4888	24.0181
Sample-5	32.2142	37.0450	28.0514	6.9879
Sample-6	29.9225	42.8904	22.8438	16.7747
Average value	28.8883	38.5301	21.8503	15.8809

(b) Statistical analysis of carbonation depth

Fig. 10. Statistical analysis of supercritical carbonation depth of SFRC.

4.3.2. Validation of the multi-phase and multi-physics coupling model

The multi-phase and multi-physics coupling model is applied to simulate the supercritical carbonation process of the SFRC. The mixing proportion and properties of the SFRC in Table 1-3 are used in the model. To eliminate the effect of random distribution of porosity on the carbonation depth, it is assumed that the porosity of the SFRC cement paste before supercritical carbonation is uniformly distributed and is 14.7%. Table 5 presents the results of numerical simulations for the mean values and the coefficient of variation of carbonation depth after supercritical carbonation. The simulations include three aspects: (1) carbonation without considering the ITZ between aggregates, steel fibers, and the cement matrix; (2) carbonation considering the ITZ between aggregates and the cement matrix only, but not between steel fibers and the cement matrix; and (3) carbonation considering the ITZ between aggregates and the cement matrix, as well as between steel fibers and the cement matrix simultaneously. By comparing the mean values of the carbonation depth and the coefficient of variation obtained from experiments and numerical simulations, it can be found that the results obtained by the numerical model are close to the experimental values, proving the validity of the model.

Table 5 shows that under supercritical CO_2 conditions, the average carbonation depth of the SFRC decreases by 5.7% to 16.6% as the volume fraction of steel fibers increases, while keeping the length to diameter ratio of the steel fibers. The increase in steel fiber volume fraction reduces plastic shrinkage cracks and lowers porosity, limiting the extension and connectivity of cracks. This limits carbonation pathways, enhances the overall density of the concrete, reduces porosity, and lowers the permeability of CO_2, thereby significantly improving the concrete's resistance to carbonation. When the volume fraction of steel fiber is fixed, the average carbonation depth of the SFRC under supercritical CO_2 conditions decreases by 5.4% to 13.1% as the length to diameter ratio of the steel fibers increases. Adding steel fibers with higher length to diameter ratio improves concrete microstructure, increases density, and reduces porosity. This, in turn, decreases the permeability of CO_2 and reduces carbonation depth.

As shown in Table 5, when examining solely the effect of the ITZ between coarse aggregate and cement matrix on carbonation depth, it is observed that the carbonation depth of the SFRC increases by 2.4% to 4.8%. When considering the effect of the ITZ between steel fiber and cement matrix alone, the carbonation depth of the SFRC is found to be increased by 0.5% to 2.3%. When evaluating the combined effects of the ITZs between the coarse aggregate and the cementitious matrix, and between the steel fiber and the cementitious matrix on carbonation depth, it is found that the carbonation depth of the SFRC is increased by 3.3% to 7.1%. The impact of the ITZ between the coarse aggregate and the cementitious matrix on the carbonation depth is found to be 2 to 6.8 times greater than that of the ITZ between the steel fibers and the cementitious matrix.

Table 5

Comparison of experimental and numerical results of supercritical carbonation depth of SFRC.

Specimens number	Test results		Simulation results					
			t_{CC}=0μm, t_{SC}=0μm		t_{CC}=100μm, t_{SC}=0μm		t_{CC}=100μm, t_{SC}=100μm	
	D_{ave} (mm)	CV_D	D_{ave} (mm)	CV_D	D_{ave} (mm)	CV_D	D_{ave} (mm)	CV_D
SFRC-L60-V0.0	32.58	0.17	32.46	0.03	33.23	0.02	33.52	0.01
SFRC-L60-V0.5	30.73	0.15	30.92	0.07	31.94	0.08	32.09	0.07
SFRC-L60-V1.0	30.17	0.11	29.72	0.43	30.9	0.36	31.3	0.42
SFRC-L60-V1.5	27.17	0.18	28.14	0.66	29.48	0.61	30.14	0.62
SFRC-L30-V1.5	28.73	0.13	29.8	0.06	30.91	0.04	31.37	0.04
SFRC-L80-V1.5	24.96	0.14	27.16	0.53	28.26	0.44	28.8	0.39

Remarks: D_{ave} and CV_D and are average carbonation depth and the coefficient of variation, respectively. t_{CC} and t_{SC} are the thicknesses of the ITZ between coarse aggregate and cementitious matrix and the ITZ between steel fibres and cementitious matrix, respectively.

4.4. Effect of volume fraction and length to diameter ratio of steel fiber on supercritical carbonation depth

To further study the evolution of carbonation depth of SFRC under supercritical CO_2 conditions with different volume fractions and length to diameter ratios of steel fibers, steel fiber volume fractions of 0%, 0.5%, 1.0%, and 1.5%, and length to diameter ratios of 30, 60, and 80 are selected. The ITZ thickness between the cement matrix, coarse aggregate, and steel fibers is uniformly set to be 100μm. The porosity of the ITZ is set to be 1.5 times that of the cement matrix. Numerical simulations of the multi-phase model for the SFRC are conducted for the above volume fractions and length to diameter ratios. For each case, three multiphase models are randomly generated and coupled with the SFRC supercritical carbonation multi-physics model. The average carbonation depth from the three models is then calculated as the numerically simulated supercritical carbonation depth of the SFRC. As shown in Fig. 11, the presence of steel fibers significantly increases the irregularity of carbonation depth, and carbonation boundary irregularities are evident at the interfaces between the cement matrix, coarse aggregate, and steel fibers.

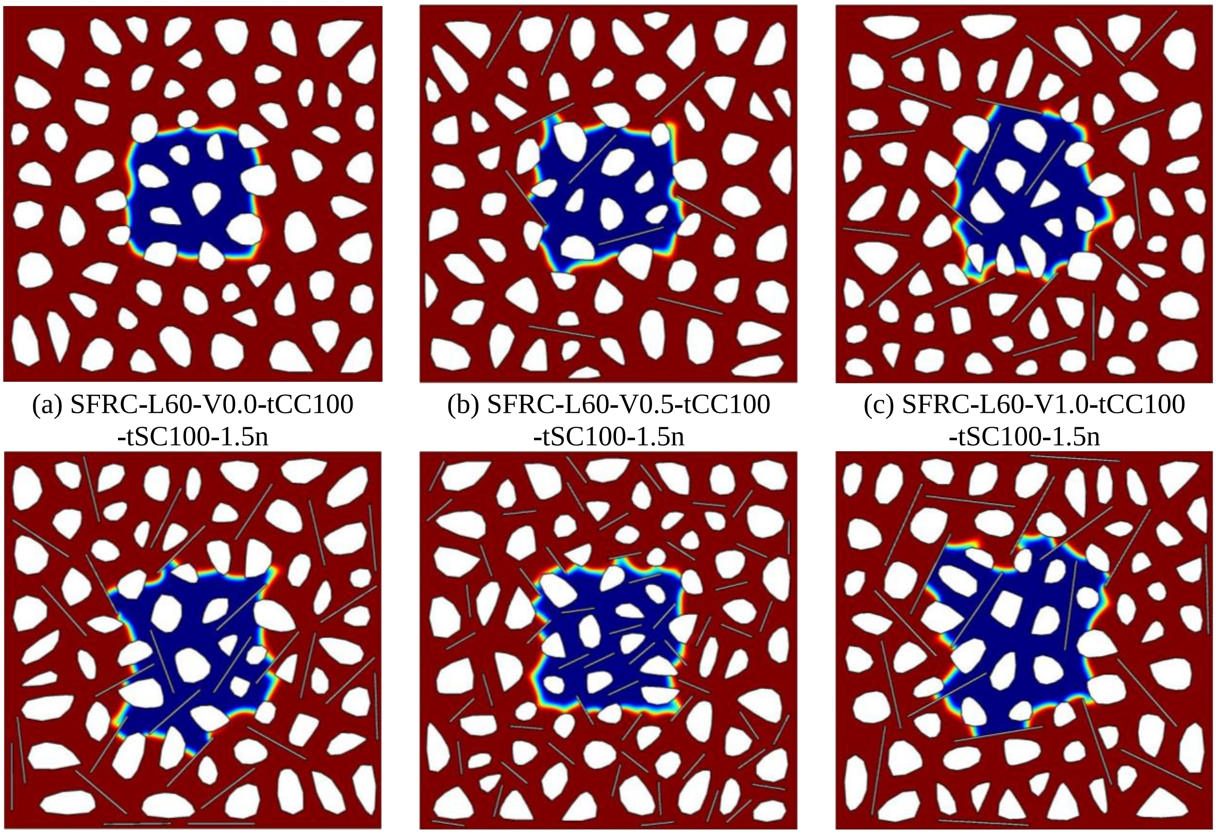

(a) SFRC-L60-V0.0-tCC100-tSC100-1.5n
(b) SFRC-L60-V0.5-tCC100-tSC100-1.5n
(c) SFRC-L60-V1.0-tCC100-tSC100-1.5n
(d) SFRC-L60-V1.5-tCC100-tSC100-1.5n
(e) SFRC-L30-V1.5-tCC100-tSC100-1.5n
(f) SFRC-L80-V1.5-tCC100-tSC100-1.5n

Fig. 11. Supercritical carbonation profiles of SFRC with different volume fraction and length to diameter ratio of steel fiber.

Note: Taking SFRC-L60-V1.5-tCC100-tSC100-1.5n as an example, tCC100 and tSC100 represent the thickness of the ITZ between the cementitious matrix and coarse aggregate, and between the cementitious matrix and steel fibers, respectively, both measuring 100 mm, 1.5n denotes the ITZ porosity, which is 1.5 times the porosity of the cementitious matrix.

The effects of different volume fractions and length to diameter ratios of steel fibers on the supercritical carbonation depth of the SFRC are shown in Fig. 12. Fig. 12(a) demonstrates the effect of various steel fiber volume fractions on the carbonation depth when the length to diameter ratio of the steel fibers is 60. It can be observed that as the volume fraction of steel fibers increases, the average carbonation depth of the SFRC gradually decreases. Specifically, for every 5% increase in the volume fraction of steel fibers, the carbonation depth decreases by an average of 3.5%. However, the standard deviation of the carbonation depth continuously increases. When the steel fiber volume fraction is not greater than 2%, the improvement in the concrete's carbonation resistance due to the increased steel fiber volume fraction is attributed to the reduction in concrete plastic shrinkage cracks and the decrease in porosity. After the carbonation reaction, the generated $CaCO_3$ fills the pores, reducing porosity and decreasing the diffusion capability of CO_2, thereby slowing down the carbonation reaction.

Fig. 12(b) shows the effect of different length to diameter ratios of steel fibers on the carbonation depth when the steel fiber volume fraction is 1.5%. It can be seen that as the length to diameter ratio of the steel fibers increases, the average carbonation depth of the SFRC gradually decreases. Specifically, for every 20-30 increase in the length to diameter ratio, the carbonation depth decreases by an average of 3.9%-4.4%. However, the standard deviation of the carbonation depth first increases and then decreases. Steel fibers with a higher length to diameter ratio bridge cracks more effectively, thus limiting crack propagation, improving the microstructure and density of the concrete, and ultimately reducing carbonation depth. Additionally, steel fibers with a larger length to diameter ratio are more likely to form a randomly distributed network structure within the concrete, effectively enhancing tensile strength in all directions and improving overall carbonation resistance.

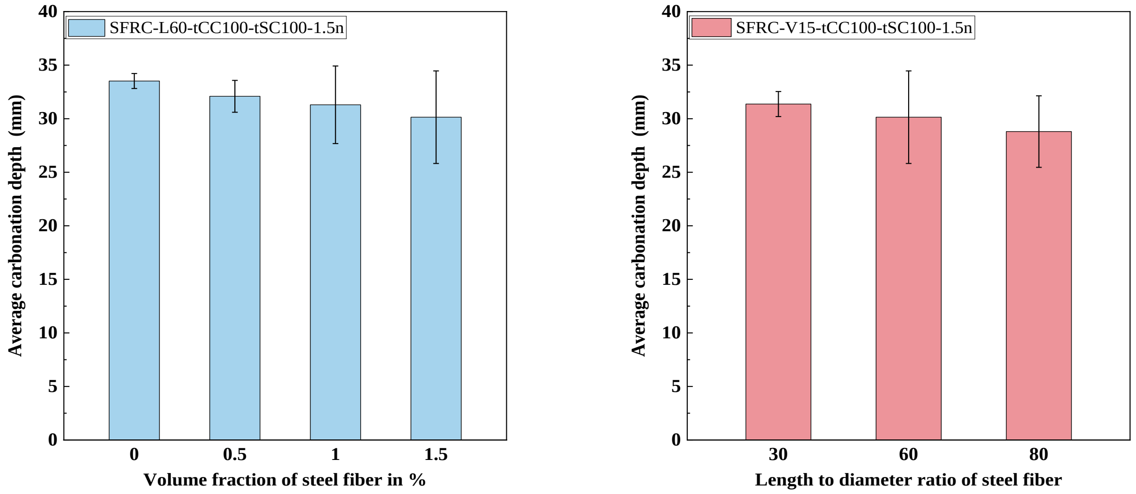

(a) Effect of volume fraction (b) Effect of length to diameter ratio

Fig. 12. Effect of volume fraction and length to diameter ratio of steel fiber on supercritical carbonation depth of SFRC.

4.5. Effect of thickness and porosity of ITZ on supercritical carbonation depth

The thickness and porosity of the ITZ between the cement matrix, coarse aggregate, and steel fibers are two significant factors that influence the carbonation process of the SFRC. Generally, the impact of ITZ on the supercritical carbonation depth of SFRC cannot be studied separately through experiments. Moreover, due to the ITZ thickness being only a few tens of micrometers, it is challenging to cast specimens with varying ITZ thicknesses to experimentally study their effect on the supercritical carbonation depth of SFRC. Given the experimental difficulties, this section uses numerical methods to investigate the influence of ITZ on the supercritical carbonation depth of SFRC. To clarify the influence of ITZ thickness and porosity between the cement matrix, coarse aggregate, and steel fibers on the carbonation depth of SFRC under supercritical CO_2 conditions, ITZ thicknesses of 0μm, 50μm, and 100μm, and ITZ to cement matrix porosity ratios of 1.0, 1.5, and 2.0 are selected. The volume fraction and length to diameter ratio of steel fiber are uniformly set to 1.5% and 80, respectively. For each ITZ thickness and porosity, three multiphase models are randomly generated and coupled with the SFRC supercritical carbonation multi-physics model. The average carbonation depth of the three models is taken as the numerically simulated supercritical carbonation depth of the SFRC. Fig. 13 shows some of the numerical simulation results, which shows the effect of the ITZ thickness and porosity between the cement matrix, coarse aggregate, and steel fibers on the distribution of SFRC supercritical carbonation depth.

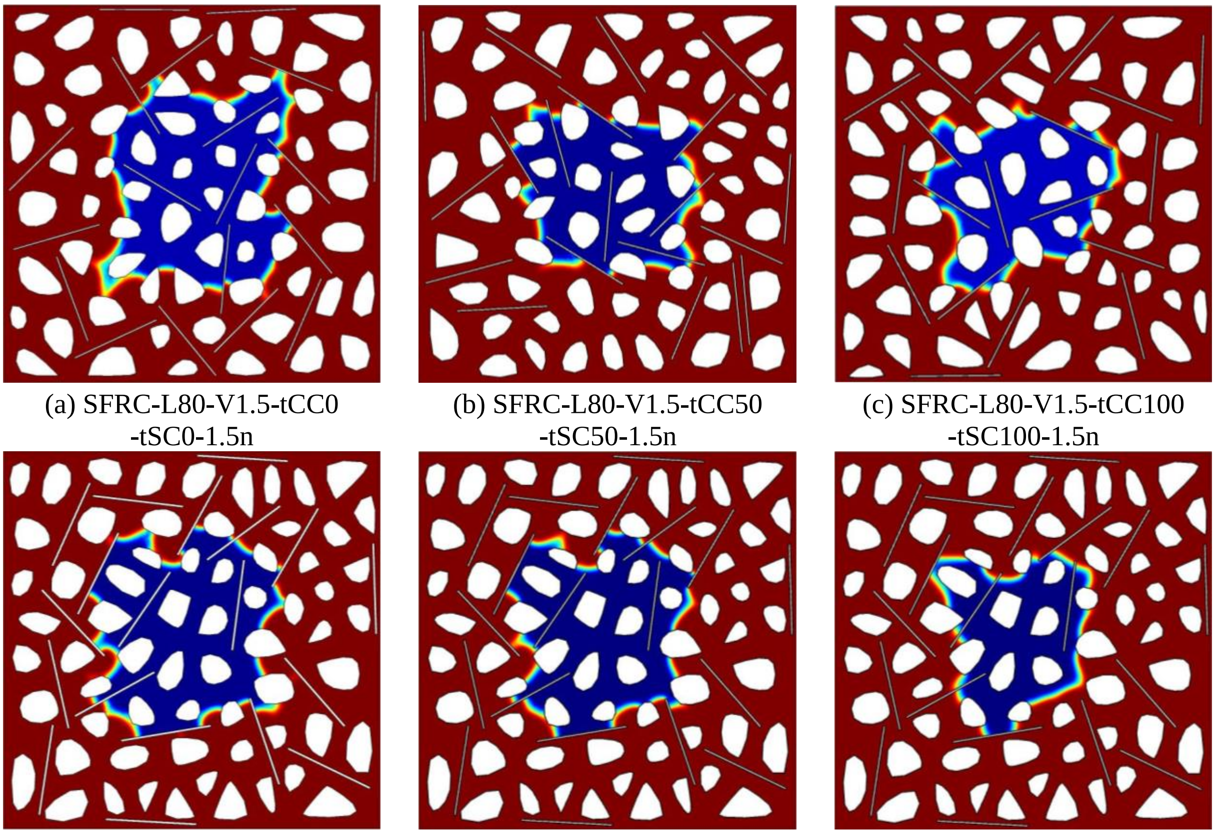

(a) SFRC-L80-V1.5-tCC0 -tSC0-1.5n
(b) SFRC-L80-V1.5-tCC50 -tSC50-1.5n
(c) SFRC-L80-V1.5-tCC100 -tSC100-1.5n
(d) SFRC-L80-V1.5-tCC100 -tSC100-1.0n
(e) SFRC-L80-V1.5-tCC100 -tSC100-1.5n
(f) SFRC-L80-V1.5-tCC100 -tSC100-2.0n

Fig. 13. Supercritical carbonation profiles of SFRC with different thickness and porosity of ITZ.

The effects of different ITZ thicknesses and porosities on the supercritical carbonation depth of the SFRC are shown in Fig. 14. Fig. 14(a) demonstrates the impact of various ITZ thicknesses on carbonation depth when the porosity ratio between the ITZ and the cement matrix is 1.5. It can be observed that as the ITZ thickness increases, the average carbonation depth gradually increases. A thicker ITZ, due to its high porosity, low alkalinity and tendency to form cracks, provides more pathways and channels for the carbonation reaction, thereby increasing the carbonation depth. The average supercritical carbonation depth for ITZ thicknesses of 50μm and 100μm increases 2.2% and 6.0%, respectively, compared to the model with an ITZ thickness of 0μm.

Fig. 14(b) shows the impact of different porosity ratios between the ITZ and the cement matrix on the carbonation depth when the ITZ thickness between the cement matrix, coarse aggregate, and steel fibers is uniformly set to 100μm. As the porosity ratio increases, the average carbonation depth of the SFRC gradually increases. Specifically, for every 0.5 increase in the porosity ratio, the carbonation depth increases by an average of 6.0% to 9.8%. An ITZ with higher porosity forms more interconnected pores and microcracks, which provides additional pathways for gases and liquids, thereby increasing the permeability of the concrete. This allows CO_2 to more easily diffuse through these pores and cracks into the concrete, where it reacts with $Ca(OH)_2$ to form $CaCO_3$, accelerating the carbonation process. Moreover, a highly porous ITZ promotes moisture migration, which is a crucial factor in the carbonation reaction. Moisture migration can carry more CO_2 into the concrete, accelerating the carbonation reaction and further increasing the carbonation depth [62]. The impact of ITZ porosity on the supercritical carbonation depth of SFRC is more pronounced compared to the impact of ITZ thickness.

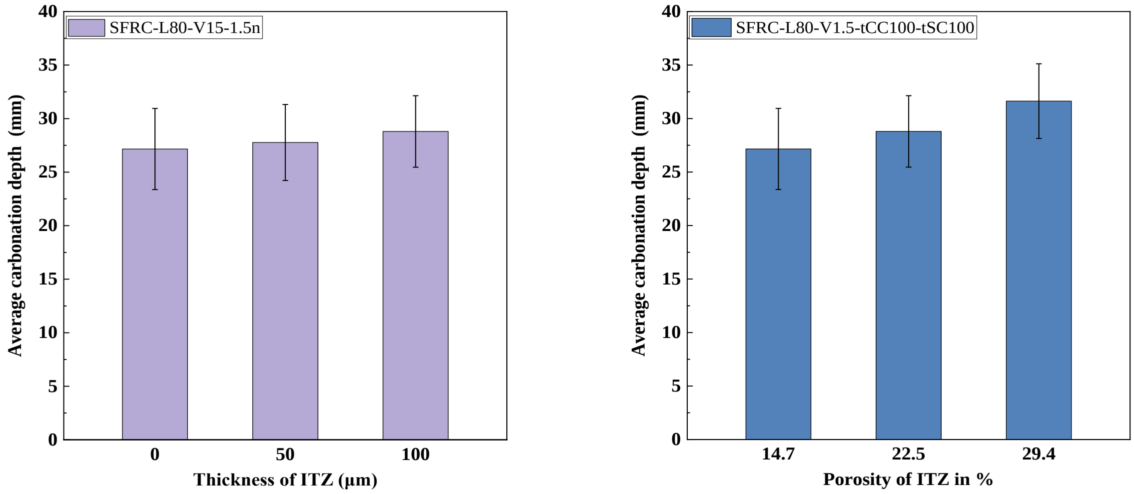

(a) Effect of thickness of ITZ (b) Effect of porosity of ITZ

Fig. 14. Effect of thickness and porosity of ITZ on supercritical carbonation depth of SFRC.

5. Conclusions

This paper presents a comprehensive experimental and numerical investigation into supercritical carbonation of SFRC. The primary conclusions are as follows:

(1) After supercritical carbonation treatment, the porosity of the SFRC is reduced by 32.3%. The ITZ between the steel fibers and the cement matrix becomes denser, and the porosity decreases. When the volume fraction of steel fibers is less than 1.5%, adding steel fibers can enhance carbonation resistance of the concrete.

(2) After supercritical carbonation, the compressive strength of SFRC increased by 25.1% ~ 42.7%

compared to that before carbonation.

(3) The proposed multi-phase and multi-physics coupling model for supercritical carbonation of SFRC can simulate random distribution of coarse aggregate, porosity, and steel fibers, along with ITZ between coarse aggregate and steel fibers and cementitious.

(4) When the volume fraction of steel fiber does not exceed 1.5%, the average supercritical carbonation depth of SFRC decreases by a maximum of 16.6% to 13.1% as the volume fraction and length to diameter ratio increases, respectively.

(5) The effect of the ITZ between the coarse aggregate and the cementitious matrix on supercritical carbonation depth of SFRC is found to be 2 to 6.8 times greater than that of the ITZ between the steel fibers and the cementitious matrix.

(6) The average carbonation depth of the SFRC gradually increases with the increase of ITZ thickness and porosity. The effect of ITZ porosity on the supercritical carbonation depth of SFRC is more pronounced compared to the impact of ITZ thickness.

Data Availability Statement

Some or all data, models, or code that support the research findings of this study are available on request.

Acknowledgements

The authors are grateful for the financial support from the National Natural Science Foundation of China (Grant No. 52308266), the China Scholarship Council (202408420235), as well as the Future City Research Institute (FCRI) Flagship Program and the Royal Society (Grant: IEC\NSFC\191350).

References

[1] Hansong Wu, Aiqin Shen, Qianqian Cheng, Yanxia Cai, Guiping Ren, Hongmei Pan, Shiyi Deng, A review of recent developments in application of plant fibers as reinforcements in concrete, J. Clean. Prod. 419 (2023) 138265, https://doi.org/10.1016/j.jclepro.2023.138265.

[2] C. Zhao, Z. Wang, Z. Zhu, Q. Guo, X. Wu, R. Zhao, Research on different types of fiber reinforced concrete in recent years: An overview, Constr. Build. Mater. 365 (2023) 130075, https://doi.org/10.1016/j.conbuildmat.2022.130075.

[3] A. Ramezanianpour, M. Esmaeili, S.-A. Ghahari, M. Najafi, Laboratory study on the effect of polypropylene fiber on durability, and physical and mechanical characteristic of concrete for application in sleepers, Constr. Build. Mater. 44 (2013) 411-418, https://doi.org/10.1016/j.conbuildmat.2013.02.076.

[4] C. Fraz˜ao, A. Camoes, ˜ J. Barros, D. Gonçalves, Durability of steel fiber reinforced self-compacting concrete, Constr. Build. Mater. 80 (2015) 155-166, https://doi.org/10.1016/j.conbuildmat.2015.01.061.

[5] M.R. Jones, A. McCarthy, Preliminary views on the potential of foamed concrete as a structural material, Mag. Concr. Res. 57 (1) (2005) 21-31, https://doi.org/10.1680/macr.2005.57.1.21.

[6] R. Bagherzadeh, A.-H. Sadeghi, M. Latifi, Utilizing polypropylene fibers to improve physical and mechanical properties of concrete, Text. Res. J. 82 (1) (2012) 88-96, https://doi.org/10.1177/0040517511420767.

[7] T.A. Söylev, T. Özturan, Durability, physical and mechanical properties of fiber reinforced concretes at low-volume fraction, Constr. Build. Mater. 73 (2014) 65-75, https://doi.org/10.1016/j.conbuildmat.2014.09.058.

[8] Rooban Chakravarthy Srikanth Venkatesan, Indubhushan Patnaikuni, Review on hybrid fiber reinforced high

performance high volume flyash concrete, Int. J. Struct. Civ. Eng. Res. 5 (1) (2016) 39-43. https://doi.org/10.18178/ijscer.5.1.39-43.
[9] H. Bolat, O. Şimşek, M. Çullu, G. Durmuş, Ö. Can, The effects of macro synthetic fiber reinforcement use on physical and mechanical properties of concrete, Compos. Part B Eng. 61 (2014) 191-198, https://doi.org/10.1016/j.compositesb.2014.01.043.
[10] L. Xu, F. Deng, Y. Chi, Nano-mechanical behavior of the interfacial transition zone between steel-polypropylene fiber and cement paste, Constr. Build. Mater. 145 (2017) 619-638, https://doi.org/10.1016/j.conbuildmat.2017.04.035.
[11] R. Serafini, S.R. Dantas, R.P. Salvador, R.R. Agra, D.A. Rambo, A.F. Berto, A.D. de Figueiredo, Influence of fire on temperature gradient and physical-mechanical properties of macro-synthetic fiber reinforced concrete for tunnel linings, Constr. Build. Mater. 214 (2019) 254-268, https://doi.org/10.1016/j.conbuildmat.2019.04.133.
[12] J. Xu, C. Wu, H. Xiang, Y. Su, Z.-X. Li, Q. Fang, H. Hao, Z. Liu, Y. Zhang, J. Li, Behaviour of ultra-high performance fibre reinforced concrete columns subjected to blast loading, Eng. Struct. 118 (2016) 97-107, https://doi.org/10.1016/j.engstruct.2016.03.048.
[13] A. Bautista, E.C. Paredes, S.M. Alvarez, et al. Welded, sandblasted, stainless steel corrugated bars in non-carbonated and carbonated mortars: a 9-year corrosion study, Corros. Sci. 102 (2016) 363-372, https://doi.org/10.1016/j.corsci.2015.10.029.
[14] J. Huang, D. Niu, Q. Fu, et al. Electrochemical and corrosion behavior of steel rebars in concrete exposed to industrial SO_2 and CO_2 environment, Constr. Build. Mater. 447 (2024) 138151, https://doi.org/10.1016/j.conbuildmat.2024.138151.
[15] M.F. Bertos, S.J.R. Simons, C.D. Hills, P.J. Carey, A review of accelerated carbonation technology in the treatment of cement-based materials and sequestration of CO_2, J. Hazard. Mater. 112 (3) (2004) 193-205, https://doi.org/10.1016/j.jhazmat.2004.04.019.
[16] J. Jerga, Physico-mechanical properties of carbonated concrete, Constr. Build. Mater. 18 (2004) 645-652, https://doi.org/10.1016/j.conbuildmat.2004.04.029.
[17] C. Liu, J. Sun, X. Tang, et al., The durability of spray steel fiber-reinforced recycled coarse aggregate concrete, Construct. Build. Mater. 412 (2024) 134731, https://doi.org/10.1016/j.conbuildmat.2023.134731.
[18] Y. Zheng, X. Lv, S. Hu, J. Zhuo, C. Wan, J. Liu, Mechanical properties and durability of steel fiber reinforced concrete: A review, J. Build. Eng. 82 (2024) 108025, https://doi.org/10.1016/j.jobe.2023.108025.
[19]P. Zhang, Q.F. Li, Durability of steel fiber-reinforced concrete containing SiO_2 nano-particles, Materials 12 (13) (2019) 2184, https://doi.org/10.3390/ma12132184.
[20] P. Zhang, Y. Yang, J. Wang, S. Hu, M. Jiao, Y. Ling, Mechanical Properties and Durability of Polypropylene and Steel Fiber-Reinforced Recycled Aggregates Concrete (FRRAC): A Review, Sustainability 12 (22) (2020) 9509, https://doi.org/10.3390/su12229509.
[21] C. Luan, X. Shi, Q. Wang, N. Utashev, R.F. Tufail, A. Maqsoom, Carbonation performances of steel fiber reinforced geopolymer concrete, Can. J. Civ. Eng. 50 (4) (2023) 294-305, https://doi.org/10.1139/cjce-2020-0797.
[22] V. Afroughsabet, L. Biolzi, T. Ozbakkaloglu, Influence of double hooked-end steel fibers and slag on mechanical and durability properties of high performance recycled aggregate concrete, Compos. Struct. 181 (2017) 273-284, https://doi.org/10.1016/j.compstruct.2017.08.086.
[23] H. Bao, M. Yu, Y. Chi, Y. Liu, J. Ye, Performance evaluation of steel-polypropylene hybrid fiber reinforced concrete under supercritical carbonation, J. Build. Eng. 43 (2021), 103159, https://doi.org/10.1016/j.jobe.2021.103159.
[24] M.S. Ammari, M. Bederina, B. Belhadj, A. Merrah, Effect of steel fibers on the durability properties of sand concrete with barley straws, Constr. Build. Mater. 264 (2020), 120689,

https://doi.org/10.1016/j.conbuildmat.2020.120689.
[25] H.L. Wu, D. Zhang, B.R. Ellis, V.C. Li, Development of reactive MgO-based Engineered Cementitious Composite (ECC) through accelerated carbonation curing, Constr. Build. Mater. 191 (2018) 23-31, https://doi.org/10.1016/j.conbuildmat.2018.09.196.
[26] M.K. Mohammed, A.R. Dawson, N.H. Thom, Carbonation of filler typed selfcompacting concrete and its impact on the microstructure by utilization of 100% CO_2 accelerating techniques, Constr. Build. Mater. 50 (2014) 508-516, https://doi.org/10.1016/j.conbuildmat.2013.09.052.
[27]F. Kaddah, H. Ranaivomanana, O. Amiri, E. Rozi`ere, Accelerated carbonation of recycled concrete aggregates: Investigation on the microstructure and transport properties at cement paste and mortar scales, J. CO_2 Util. 57 (2022), 101885, https://doi.org/10.1016/j.jcou.2022.101885.
[28] J. Shen, P. Dangla, M. Thiery, Reactive transport modeling of CO_2 through cementitious materials under CO_2 geological storage conditions, Int. J. Greenh. Gas. Control 18 (2013) 75-87, https://doi.org/10.1016/j.ijggc.2013.07.003.
[29] D.X. Xuan, B.J. Zhan, C.S. Poon, Assessment of mechanical properties of concrete incorporating carbonated recycled concrete aggregates, Cem. Concr. Compos. 65 (2016) 67-74, https://doi.org/10.1016/j.cemconcomp.2015.10.018.
[30] J. Zhang, C. Shi, Y. Li, X. Pan, C.S. Poon, Z. Xie, Influence of carbonated recycled concrete aggregate on properties of cement mortar, Constr. Build. Mater. 98 (2015) 1-7, https://doi.org/10.1016/j.conbuildmat.2015.08.087.
[31] S. Kou, B. Zhan, C.S. Poon, Use of a CO_2 curing step to improve the properties of concrete prepared with recycled aggregates, Cem. Concr. Compos. 45 (2014) 22-28, https://doi.org/10.1016/j.cemconcomp.2013.09.008.
[32] R. Hay, K. Celik, Accelerated carbonation of reactive magnesium oxide cement (RMC)-based composite with supercritical carbon dioxide ($scCO_2$), J. Clean. Prod. 248 (2020), 119282, https://doi.org/10.1016/j.jclepro.2019.119282.
[33] C.A. Garcia-Gonzalez, A. Hidalgo, C. Andrade, M.C. Alonso, J. Fraile, A.M. Lopez-Periago, C. Domingo, Modification of composition and microstructure of Portland cement pastes as a result of natural and supercritical carbonation procedures, Ind. Eng. Chem. Res. 45 (14) (2006) 4985-4992, https://doi.org/10.1021/ie0603363.
[34] X. Zha, H. Wang, P. Xie, C. Wang, P. Dangla, J. Ye, Leaching resistance of hazardous waste cement solidification after accelerated carbonation, Cem. Concr. Compos. 72 (2016) 125-132, https://doi.org/10.1016/j.cemconcomp.2016.06.001.
[35] X. Zha, J. Ning, M. Saafi, L. Dong, Effect of supercritical carbonation on the strength and heavy metal retention of cement-solidified fly ash, Cem. Concr. Res. 120 (2019) 36-45, https://doi.org/10.1016/j.cemconres.2019.03.005.
[36] M.A. Venhuis, E.J. Reardon, Vacuum method for carbonation of cementitious wasteforms, Environ. Sci. Technol. 35 (20) (2001) 4120-4125, https://doi.org/10.1021/es0105156.
[37] J.B. Rubin, J.W. Carey, C. Taylor, Enhancement of cemented waste forms by supercritical CO_2 carbonation of standard portland cements (1997) 473-478,
[38] H. Bao, X.u. Gang, Y.u. Min, Q. Wang, R. Li, M. Saafi, J. Ye, Evolution of ITZ and its effect on the carbonation depth of concrete under supercritical CO_2 condition, Cem. Concr. Compos. 126 (2022), 104336, https://doi.org/10.1016/j.cemconcomp.2021.104336.
[39] C.A. García-González, N. el Grouh, A. Hidalgo, J. Fraile, A.M. López-Periago, C. Andrade, C. Domingo, New insights on the use of supercritical carbon dioxide for the accelerated carbonation of cement pastes, J. Supercrit. Fluids 43 (2008) 500-509, https://doi.org/10.1016/j.supflu.2007.07.018.
[40] P. Purnell, N.R. Short, C.L. Page, Super-critical carbonation of glass-fibre reinforced cement. Part 1:

mechanical testing and chemical analysis, Compos. A Appl. Sci. Manuf. 32 (2001) 1777-1787, https://doi.org/10.1016/S1359-835X(01)00019-7.
[41] X. Zha, H. Wang, G. Feng, Effects of supercritical carbonation on the property and pore structure of cement-based materials, J. Harbin I Technol. 11 (2014) 52-57 (in Chinese).
[42] T. Hartmann, P. Paviet-Hartmann, J. Rubin, M. Fitzsimmons, K. Sickafus, The effect of supercritical carbon dioxide treatment on the leachability and structure of cemented radioactive waste-forms, Waste Manage. 19 (5) (1999) 355-361, https://doi.org/10.1016/S0956-053X(99)00138-5.
[43] L.F. Carrasco, J. Rius, C. Miravitlles, Supercritical carbonation of calcium aluminate cement, Cem. Concr. Res. 38 (2008) 1033-1037, https://doi.org/10.1016/j.cemconres.2008.02.013.
[44] S.F. Santos, R. Schmidt, A.E. Almeida, G.H. Tonoli, H. Savastano, Supercritical carbonation treatment on extruded fibre-cement reinforced with vegetable fibres, Cement Concr. Compos. 56 (2015) 84-94, https://doi.org/10.1016/j.cemconcomp.2014.11.007.
[45] H.O. Shin, J.M. Yang, Y.S. Yoon, D. Mitchell, Mix design of concrete for prestressed concrete sleepers using blast furnace slag and steel fibers, Cem. Concr. Compos. 74 (2016) 39-53, https://doi.org/10.1016/j.cemconcomp.2016.08.007.
[46] X. Zha, M. Yu, J. Ye, G. Feng, Numerical modeling of supercritical carbonation process in cement-based materials, Cem. Concr. Res. 72 (2015) 10-20, https://doi.org/10.1016/j.cemconres.2015.02.017.
[47] P. Smarzewski, Influence of basalt-polypropylene fibres on fracture properties of high performance concrete, Compos. Struct. 209 (2019) 23-33, https://doi.org/10.1016/j.compstruct.2018.10.070.
[48] Min Yu, Hao Bao, Jianqiao Ye, Yin Chi, The effect of random porosity field on supercritical carbonation of cement-based materials, Constr. Build. Mater. 146 (2017) 144-155, https://doi.org/10.1016/j.conbuildmat.2017.04.060.
[49] China National Standards, Specification for mix proportion design of ordinary concrete, JGJ 55−2011. (2011) (in Chinese).
[50] China National Standards, Standard test methods for fiber reinforced concrete, CECS 13: 2009. (2009) (in Chinese).
[51] H. Bao, M. Yu, Y. Liu, J. Ye, Experimental and statistical study on the irregularity of carbonation depth of cement mortar under supercritical condition, Constr. Build. Mater. 174 (2018) 47-59, https://doi.org/10.1016/j.conbuildmat.2018.04.100.
[52] H. Bao, M. Yu, L. Xu, M. Saafi, J. Ye, Experimental study and multi-physics modelling of concrete under supercritical carbonation, Constr. Build. Mater. 227 (2019) 116680, https://doi.org/10.1016/j.conbuildmat.2019.116680.
[53] L. Xu, F. Deng, Y. Chi, Nano-mechanical behavior of the interfacial transition zone between steel-polypropylene fiber and cement paste, Constr. Build. Mater. 145 (2017) 619-638, https://doi.org/10.1016/j.conbuildmat.2017.04.035.
[54] M. Zhou, X.J. He, H.Y. Wang, C. Wu, J. He, B.Y. Wei, Mechanical properties and microstructure of ITZs in steel and polypropylene hybrid fiber-reinforced concrete, Constr. Build. Mater. 415 (2024) 135119, https://doi.org/10.1016/j.conbuildmat.2024.135119.
[55] V. Baroghel-Bouny, M. Thi´ery, X. Wang, Modelling of isothermal coupled moisture–ion transport in cementitious materials, Cem. Concr. Res. 41 (8) (2011) 828-841, https://doi.org/10.1016/j.cemconres.2011.04.001.
[56] I.O. Yaman, N. Hearn, H.M. Aktan, Active and non-active porosity in concrete part I: experimental evidence, Mater. Struct. 35 (2) (2002) 102-109, https://doi.org/10.1007/BF02482109.
[57] Mingfeng Lei, Linghui Liu, Ziwei Hu, et al. Strain localization mechanisms in steel fiber-reinforced self-compacting concrete under compression: An experimental study, Journal of Building Engineering. 99 (2025) 111583, https://doi.org/10.1016/j.jobe.2024.111583.

[58] Lei Gu, Dhanendra Kumar, Cise Unluer, et al. Investigation of non-uniform carbonation in strain-hardening magnesia composite (SHMC) and its impacts on fiber-matrix interface and fiber-bridging properties, Cement and Concrete Composites. 153 (2024) 105726, https://doi.org/10.1016/j.cemconcomp.2024.105726.

[59] Chen Lin, Terje Kanstad, Stefan Jacobsen, Guomin Ji, Bonding property between fiber and cementitious matrix: A critical review, Construction and Building Materials. 378 (2023) 131169, https://doi.org/10.1016/j.conbuildmat.2023.131169.

[60] Q. Chen, H. Zhu, Z. Yan, et al., A multiphase micromechanical model for hybrid fiber reinforced concrete considering the aggregates and ITZ effects, Constr. Build. Mater. 114 (2016) 839-850, https://doi.org/10.1016/j.conbuildmat.2016.04.008.

[61] B. Wu, G. Ye, Development of porosity of cement paste blended with supplementary cementitious materials after carbonation, Constr. Build. Mater. 145 (2017) 52-61, https://doi.org/10.1016/j.conbuildmat.2017.03.176.

[62] P. Van den Heede, C. Thiel, N. De Belie, Natural and accelerated carbonation behaviour of high-volume fly ash (HVFA) mortar: effects on internal moisture, microstructure and carbonated phase proportioning, Cem. Concr. Compos. 113 (2020), 103713, https://doi.org/10.1016/j.cemconcomp.2020.103713.